Multiple scattering of high-frequency seismic waves in the deep Earth: PKP precursor analysis and inversion for mantle granularity.

Ludovic Margerin, G. Nolet

Multiple scattering of high-frequency seismic waves in the deep Earth: *PKP* precursor analysis and inversion for mantle granularity

L. Margerin

Laboratoire de Géophysique Interne et Tectonophysique, CNRS, Joseph Fourier University, Grenoble, France

G. Nolet

Department of Geosciences, Princeton University, Princeton, New Jersey, USA

Received 17 February 2003; revised 19 June 2003; accepted 18 July 2003; published 6 November 2003.

[1] We apply the theory of radiative transfer to invert for the small-scale structure of the mantle, by fitting mean amplitude envelopes of precursors to *PKP* in the time domain. The data set previously used by *Hedlin and Shearer* [2000] have been augmented with new deep events from the 1997–2000 period, thereby doubling the number of high-quality records selected for this study. Regional and global average amplitudes are measured in six bins covering the 124–142° epicentral distance range. The inversion focuses on stacks for strongly scattering wave paths only and aims to determine the depth extent and power spectrum of the mantle heterogeneities that cause the scattered signals. We find that the restriction of scatterers to the D'' layer is incompatible with observations. Instead, whole mantle scattering models reproduce with reasonable accuracy the time dependence of precursors, in agreement with previous findings. Exponential correlations predict a spatial rate of decay of the precursor amplitude which is much faster than observed. Thus we are led to propose a new model of mantle heterogeneity, richer in small-scale than exponential media, that fits uniformly the data. An analytic form of the correlation function and power spectrum of our new model is given explicitly. It is shown that the precise length scale of heterogeneities is fundamentally unresolvable because of the limited range of observations. The perturbations in *P* wave velocities required to fit the data are only of order 0.1–0.2%, which is more than 1 order of magnitude less than found in previous studies. *INDEX TERMS:* 7203 Seismology: Body wave propagation; 7207 Seismology: Core and mantle; 7260 Seismology: Theory and modeling; *KEYWORDS:* multiple scattering, radiative transfer, heterogeneity, power spectrum, lower mantle, D″ layer

Citation: Margerin, L., and G. Nolet, Multiple scattering of high-frequency seismic waves in the deep Earth: *PKP* precursor analysis and inversion for mantle granularity, *J. Geophys. Res.*, *108*(B11), 2514, doi:10.1029/2003JB002455, 2003.

1. Introduction

[2] In recent years, seismic tomography has revealed in great detail the structure of the Earth interior and has provided answers to fundamental geodynamical questions. For example, the discovery of slab penetration through the 670-km discontinuity has ruled out the strict two-layer mantle convection hypothesis, and has raised numerous questions pertaining to the interpretation of geochemical observations. In particular, the existence of at least four isotopically distinct reservoirs asks for a deeper understanding of the spatial distribution of chemical heterogeneities. The characterization and mapping of heterogeneous structures at all scales is more than ever a challenging issue for seismology.

[3] It is striking that most high-resolution global tomography studies, while of immense and still growing importance in geodynamics, rely solely on the ray interpretation of travel times of seismogram phases. This calls for a few comments. First, because ray theory is an infinite frequency approximation, it cannot take into account wave front healing and diffraction, thereby ignoring the fact that there are fundamental limitations in resolution of tomographic images based on seismic travel times only [*Nolet and Dahlen*, 2000]. *Dahlen et al.* [2000] and *Hung et al.* [2000] showed that the coupling of Born and ray theory improves the recovery of velocity anomalies that are masked by the effect of wave front healing. Second, delay time tomography ignores the vast amount of information potentially contained in wave amplitudes. In practice, the inversion of seismic amplitudes is difficult because amplitudes are extremely sensitive to geometric effects (focusing/defocusing), scattering, intrinsic absorption, source radiation, and multiple crustal reflections. Finally, the analysis of scattered waves themselves can potentially provide important information on the statistical properties of small-scale

0148-0227/03/2003JB002455$09.00

heterogeneity that is fundamentally unresolvable by tomographic analysis. The latter approach is the topic of this paper.

[4] High-frequency (>1 Hz) seismic waves travel distances equivalent to a thousand or more wavelengths through the Earth and are likely to encounter numerous inhomogeneities. Along the way, ray tubes are not only bent by velocity gradients, but an important part of their energy is transferred to the whole sphere of space directions. This is evidenced by the existence of long-lasting codas following, also sometimes preceding, seismic phases. Astronomers face a very similar problem when they analyze the light that has propagated through planetary atmospheres. In this field, the fruitfulness of statistical approaches has long been recognized. Because atmospheres are so complex at the wavelength scale, the stochastic theory of radiative transfer (or transport theory) has been developed to interpret average properties of scattered signals. For example, *Hansen and Hovenier* [1974] predicted the composition of Venus atmosphere using transport theory more than 20 years before it was confirmed by direct observations.

[5] In this paper, we will show how statistical properties of small-scale fluctuations in the Earth mantle can be inverted for using transport theory. Much of our investigations have been stimulated by the pioneering works of *Cormier* [1995, 1999] and *Hedlin et al.* [1997] and *Hedlin and Shearer* [2000], who demonstrated the feasibility of modeling the root-mean-square (RMS) amplitudes of high-frequency seismic signals using Born approximation. Remarkably, Hedlin and his coworkers found evidence that the Earth mantle is filled with small-scale structures (of the order 10 km), with about 1% perturbations or more. The companion paper by *Margerin and Nolet* [2003] (hereinafter referred to as RT-I) formulated the transport theory of elastic waves developed by *Weaver* [1990] and *Ryzhik et al.* [1996] in a seismological context. Transport theory enables the modeling of full seismogram envelopes and incorporates in a rigorous way arbitrarily high orders of scattering. Although first derived by physicists using Feynman's diagrammatic methods [*Barabanenkov et al.*, 1972], mathematicians [*Ryzhik et al.*, 1996] have shown that in a regime of separation of scales, radiative transfer theory is an exact consequence of the wave equation.

[6] RT-I presented in details a Monte Carlo method of solution of the transport equation and showed in a series of numerical tests that for fluctuations typically less than 0.5%, transport and Born theories are essentially equivalent. However, in whole mantle scattering models with large fluctuations (1% or more) as proposed by *Hedlin et al.* [1997], the two theories diverge very significantly. To state it in a few words, we found that Born theory wrongly predicts the spatiotemporal distribution of energy, because of its inability to take multiple scattering into account. It is intuitively appealing to propose strong multiple scattering in a heterogeneous D'' layer as an alternative interpretation for Hedlin et al's observations. We therefore undertook a new experimental and theoretical investigation of *PKP* precursors amplitude in the light of our modeling results [*Margerin and Nolet*, 2003].

[7] The mechanism of generation of the precursors has been investigated by a number of authors in the past and is now fairly well understood. They were first observed by *Bolt* [1962], who interpreted them in terms of complex one-dimensional velocity structures at the inner core outer core boundary. This early explanation was ruled out in the seventies by several array analyses by *Cleary and Haddon* [1972], *Doornbos and Husebeye* [1972] and *King et al.* [1974], who put forward scattering by lower mantle inhomogeneities as the mechanism of precursor generation. This is schematically depicted in Figure 1. As they cross the core-mantle boundary, $PKP_{ab,bc}$ waves interact with small-scale fluctuations of the lower mantle and deflect energy into the shadow zone. Simple ray-tracing shows that these scattered waves can arrive up to 18 s before the main PKP_{df} phase, in agreement with observations. The interest in *PKP* precursors is strongly connected to the fact that they are not contaminated by the coda of other phases and therefore constitute a unique opportunity to have direct access to the presence of small-scale heterogeneity at depth.

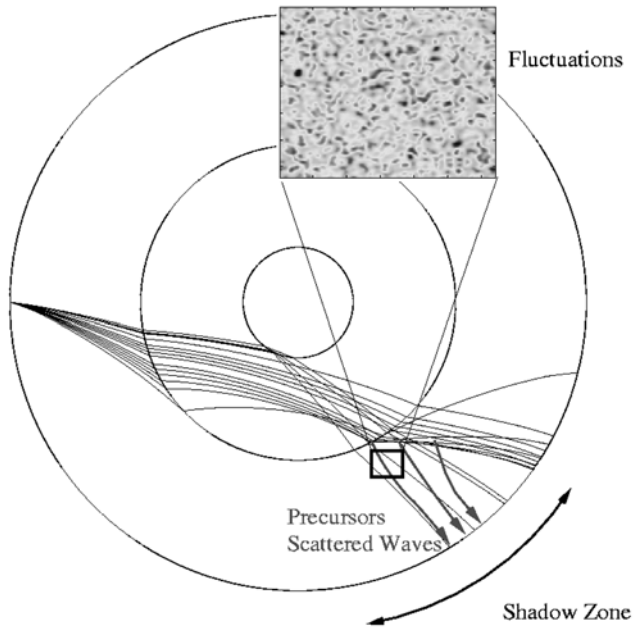

Figure 1. Mechanism of generation of *PKP* precursors. A few rays (in black) show the propagation paths of the different core phases. Arrows denote scattered $PKP_{ab,bc}$ waves in the lower mantle arriving before PKP_{df}. Although not represented, receiver-side scattering would explain the precursors equally well.

[8] The mapping of scatterers inside the mantle has been a topic of heated debate and controversy. *Doornbos and Vlaar* [1973] were the first to promote a whole mantle scattering hypothesis, but were contradicted one year later by *Haddon and Cleary* [1974], who defended the D'' hypothesis instead. Proponents defended each model in a series of publications [*Doornbos*, 1976, 1978; *Husebeye et al.*, 1976] until interest in the topic started to decline at the end of the 1970s. New modeling approaches [*Cormier*, 1995, 1999; *Hedlin et al.*, 1997; *Hedlin and Shearer*, 2000; *Shearer et al.*, 1998] have recently shed new light on the old observations. Here we propose a different modeling approach based on the theory of radiative transfer and apply it to an improved and more selective data set. An

important goal of our study is to relate the range time dependence of precursor amplitudes measured at the surface of the Earth to the power spectrum of mantle heterogeneities.

[9] Before going to our inversion procedure and results, section 2 is devoted to the method of selection and analysis of data.

2. Data Selection

[10] For this study we used the data selected by *Hedlin and Shearer* [2000] for the period 1988–1997, augmented with new data from deep events (>80 km) up to December 2000. For the period 1998–2000, we inspected all deep events irrespective of their source mechanism, with magnitude 6 or higher recorded by the Global Seismic Network (GSN) network for three promising source regions in South America, Tonga-Fiji, and Indonesia, as well as many others. Since our main aim is to investigate the temporal, spectral, and amplitude characteristics of strong precursors, we have only selected seismograms with a high signal-to-noise (S/N) ratio. In rejecting seismograms with no clear indications of scattered signals we differ from the approach taken by *Hedlin et al.* [1997], who average over all wave paths. Obviously, low- noise seismograms that show no precursor contain significant information about the lateral variability of the region where the precursors occur [*Hedlin and Shearer*, 2000]. However, for an adequate investigation of lateral variability, we first need to establish with sufficient degree of certainty whether precursors originate in the D'' layer or in a larger region of the lower mantle, and it is this question in particular that we address in the present study.

[11] Our data set comprises 357 observations of precursors. 152 of these were classified (subjectively) as "doubtful," meaning that a change in the character of the seismogram before the onset was detected but with a signal-to-noise ratio before filtering of the order of 1 or worse. The remaining 205 seismograms had an unambiguous precursor; 103 of these came from *Hedlin et al.*'s [1997] original data set, so we effectively doubled the number of precursors visible by eye (this increase was made possible by the rapid expansion of the GSN in the last few years). The S/N ratio, the duration of the precursor, and the distribution over epicentral distance for the 205 reliable precursors are summarized in Figure 2. The duration of the precursor is defined as the time between the observed onset of the precursor and the (hand-picked) arrival time of PKP_{df}. The S/N ratio shown here is for unfiltered seismograms and was determined by computing the RMS amplitudes of the signal in time windows before and after the precursor onset equal in length to the precursor duration. We note that the S/N ratio often greatly improves when data are high-pass filtered to remove the microseismic noise. Figure 2 allows us already to make an important observation. The parabola-shaped curve in Figure 2 denotes the earliest possible onset for a precursor generated at the core-mantle boundary (CMB). Shorter durations may not automatically be interpreted as evidence for a scatterer that is located far away from the CMB, as the onset of the precursor is often difficult to pick when the S/N ratio is low. Moreover, these late arrivals may be well explained by scatterers located near the CMB but off the great circle path.

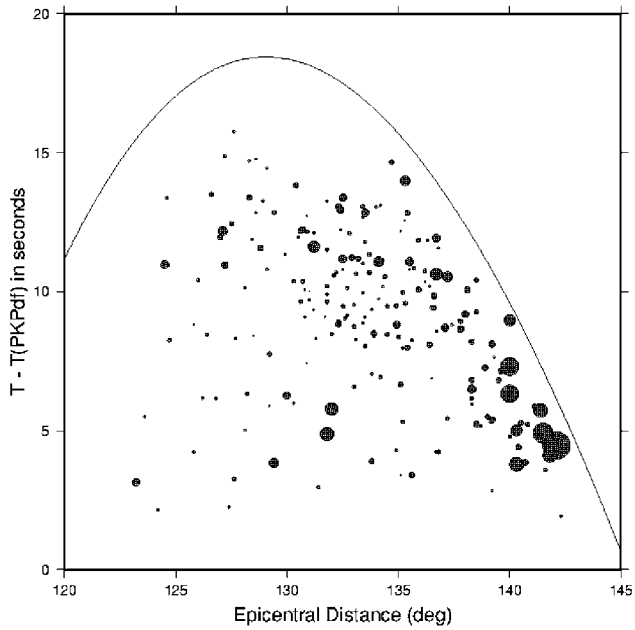

Figure 2. Signal-to-noise (S/N) ratio from the unfiltered seismograms for the 205 clearly visible precursors selected for this study, in a plot of the duration of PKP_{df} precursors as a function of epicentral distance. The onset of PKP_{df} precursors was determined by eye from velocity seismograms high passed at 0.4 Hz. Similarly, the onset of PKP_{df} was determined by eye from unfiltered velocity seismograms. The size of the symbols is proportional to the S/N ratio between precursor and microseismic noise, measured over the full frequency band from time windows of equal length to the precursor duration, just before and after the onset of the precursor. This S/N ratio varies linearly from 10 for the largest symbol to slightly less than 1 for the smallest dots. Note that the S/N ratio increases significantly after filtering out the microseismic noise (see Figure 3). The parabolic line denotes the earliest possible onset for a precursor to arrive if the scatterer is located at the core-mantle boundary. Note that no precursors are observed at any earlier times, precluding a location of the scatterer below the CMB.

However, it is intriguing to see quite a few observations with a high S/N ratio and a duration far shorter than predicted by a scatterer located in or near D''. No precursors arrive before the theoretically predicted time for a scatterer located at the CMB. This seems to rule out the location of scatterers in the fluid core itself, such as might be expected if significant "upward" sedimentation takes place inside the fluid core, as suggested by *Buffett et al.* [2000]. A similar observation was made by *Shearer et al.* [1998].

[12] In order to determine the optimal spectral window for an analysis of the precursors, we have stacked the amplitude spectra of the 45 precursors with an unfiltered S/N ratio larger than 2. The spectra are shown in Figure 3. The thin line of low amplitude is the spectrum of the microseismic noise before the arrival of the precursor, which is clearly below the amplitude spectrum of the signal in the precursor window (bold line). The dashed line in

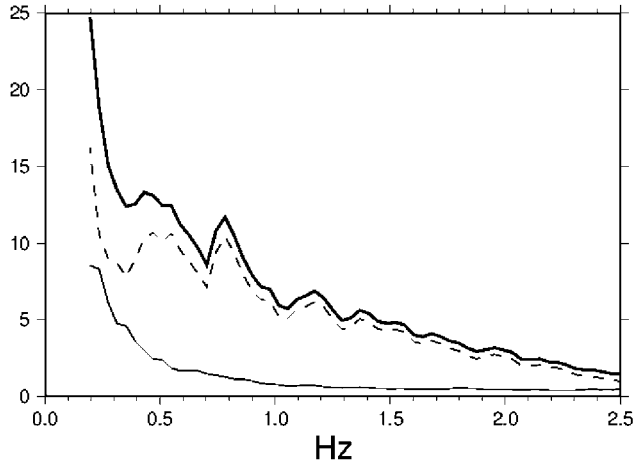

Figure 3. Stacked velocity spectra (bold line) for 45 PKP_{df} precursor signals at epicentral distances 124.5–142.6°. The precursors were selected on a S/N ratio between the precursors and the preceding microseismic noise larger than 2. The stack uses weights inversely proportional to the microseismic noise energy. Thin line denotes stacked spectrum for the microseismic noise in a time window just before the precursor of the same length as the precursor. Dashed line denotes precursor spectrum minus noise spectrum.

Figure 3 was obtained by subtracting the noise from the precursor spectrum. This clearly shows that the largest S/N ratios for the precursors are obtained for frequencies above about 0.4 Hz, and gives us confidence that very few if any precursors constitute misidentified bursts of microseismic noise. In the following, our analysis of the precursors and their envelopes is therefore based on seismograms that are band passed between 0.4 and 2.5 Hz.

[13] Figure 4 shows the source-station pairs for the 205 precursors with high S/N ratio. Since PKP_{df} is a very steeply dipping ray, the points of impact at the CMB are located near the endpoints of the rays. Even a casual observer inspecting our data would soon notice that several stations occur preferentially in our set, in particular, ARU in Russia, with 33 of the 205 seismograms, ABKT in Turkmenistan (20 seismograms), SPA at the South Pole (17 seismograms), OBN in Russia (15 seismograms), ANMO in New Mexico (15 seismograms), CCM in Missouri (13 seismograms), RAYN in Saudi Arabia (12 seismograms), and WRAB in Australia (11 seismograms) all contribute more than 10 seismograms to our data set. This total number of precursors is the result of many factors, such as the noise level and the start date of operation, but a high frequency of occurrence in these stations is nevertheless a clear indication that selected regions inside the Earth are especially favorable for the generation of PKP_{df} precursors. These might either be below the particular station, or, as in the case of ARU, OBN, and ABKT which have similar azimuth from the source region in Tonga, below the earthquake. Some examples of precursors with a good S/N ratio are shown in Figure 5.

3. Precursor Envelopes

[14] Before presenting the experimental results, we devote some space to reviewing fundamental ideas of radiative

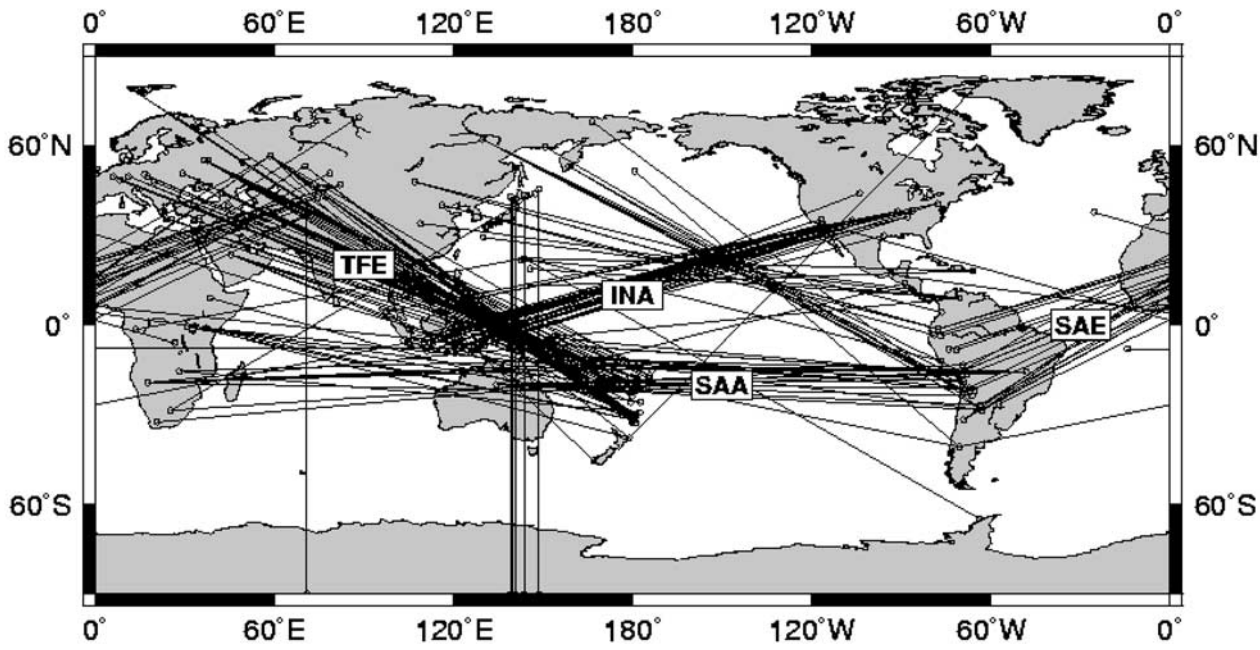

Figure 4. Source-receiver combinations for the 205 seismograms used for the global stacks of low-noise/high-amplitude precursor envelopes in this study. Four densely populated corridors, from Tonga-Fiji to Eurasia (TFE), South America to Eurasia (SAE), Indonesia to North America (INA), and South America to Australia (SAA), have been selected for regionalized stacks. Sources and receivers have been connected by straight lines (not great circles) to show the grouping of the four corridors more clearly.

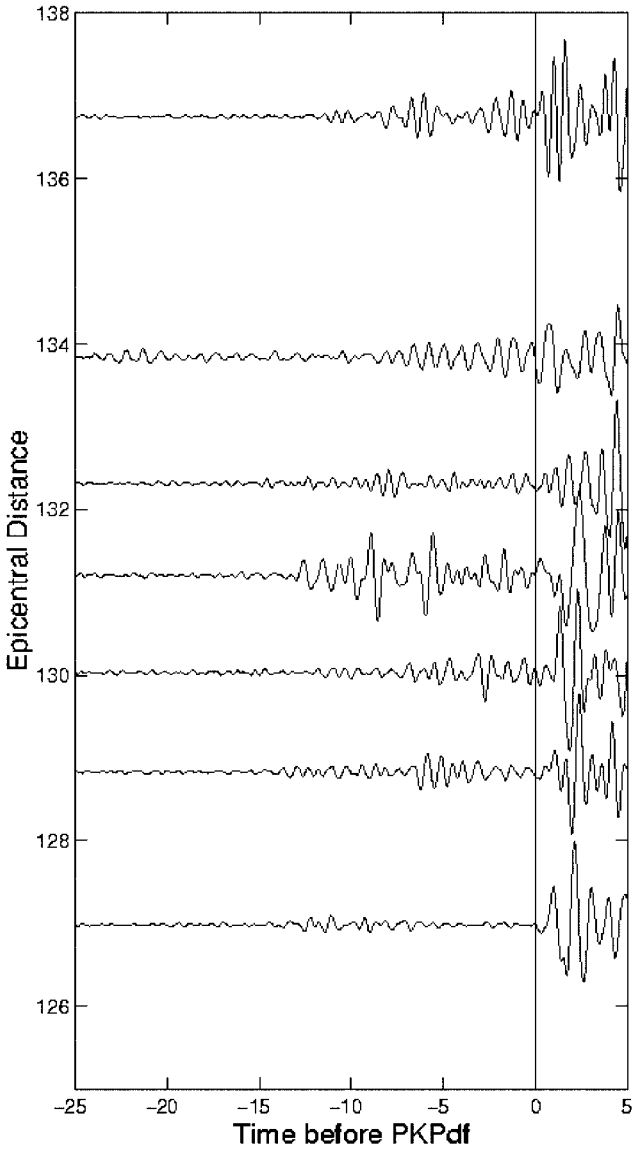

Figure 5. Examples of clearly visible PKP_{df} precursors in the epicentral distance range 124°–142°. This is a composite plot of different events.

transfer and to establish the connection between the theory and the observations. In Figure 5, we show sample records of *PKP* precursors at different epicentral distances, which illustrates the complexity of the high-frequency teleseismic wave field. Thus a complete wiggle-to-wiggle fit of these data is clearly out of reach. Instead of looking at the whole wave field, it is possible to analyze the data envelopes in a narrow frequency band, as is customary in crustal seismology [see, e.g., *Sato and Fehler*, 1998]. As illustrated in Figure 6, the RMS amplitude of the precursors is smooth and varies on a much slower timescale than the central frequency of the waves. In this particular regime where the fast oscillations of the wave field are clearly separated from the slow evolution of the energy envelope, it is possible to derive a transport or radiative transfer equation governing the mean intensity of the wave field. This equation has been presented and discussed in a seismological context in RT-I but the basic physical assumptions are recalled hereafter. Radiative transfer relies on the idea that the seismic wave field u at a given point is a sum of individual plane waves having slowly varying amplitudes A and phases ϕ:

$$u(t) = \sum_j A_j(t) e^{i\left(\omega t + \phi_j(t)\right)}, \tag{1}$$

where ω is the central frequency of the waves and j is used to label each wave. It is important to note that while the field u varies very rapidly, the amplitude A changes on a much longer timescale $t \gg 1/\omega$ and constitutes a robust observation. The short-period coda of crustal earthquakes is another excellent illustration of this separation of timescales [*Sato and Fehler*, 1998]. We will further assume that the field complexity reflects the random or disordered character of the medium and that the different incoming plane waves have visited different random inhomogeneities. Thus the ϕ_j can be considered as uncorrelated random variables. As a consequence, the average field intensity $I(t)$ is just the sum of the contributions of each individual plane wave:

$$I = C \sum_j \left\langle A_j^2 \right\rangle, \tag{2}$$

where C is a scaling constant depending on the wave type (electromagnetic, elastic, etc.), and the angle brackets denote an ensemble averaging. As is customary, the RMS amplitude will be defined as the square root of I. Equation (2) highlights the fact that intensities (rather than amplitudes) are additive in disordered media. Note that when the separation of timescales is violated, interferences persist and transfer theory breaks down. The additivity of intensities and the separation of timescales are fundamental ideas of the theory of radiative transfer. Although we have resorted to rather heuristic arguments, the conditions of application of transport theory have been theoretically well established [*Apresyan and Kravtsov*, 1996; *Rytov et al.*, 1989a, 1989b]. It is important to note that the angle brackets usually have a different meaning in the theory and in the observations. The rigorous definition of the mean intensity involves an ensemble average over different configurations of the random medium. In practice, we can never obtain this type of averaging because the disorder inside the Earth is quenched on the timescale of our observations. In this sense, there is only one configuration. In practice, we replace the ensemble average by an average over different paths.

[15] After selecting the high-amplitude, low-noise precursors and 0.4–2.5 Hz band-pass filtering, envelopes were calculated in Seismic Analysis Code (SAC). Thereby, we rejected the 152 records that were classified as doubtful. The envelopes were smoothed with a running average window of 4 s length, which is about 6 times the dominant period of the scattered waves. The raw stacked envelopes are still somewhat oscillatory. These oscillations decrease with the number of seismograms in the stack and are therefore not likely a violation of our assumption that timescales are separable. We note that the adopted smoothing window is short enough to minimize effects on the sharpness of the onset while greatly damping the high-frequency oscillations. We divided the envelopes over six 3°

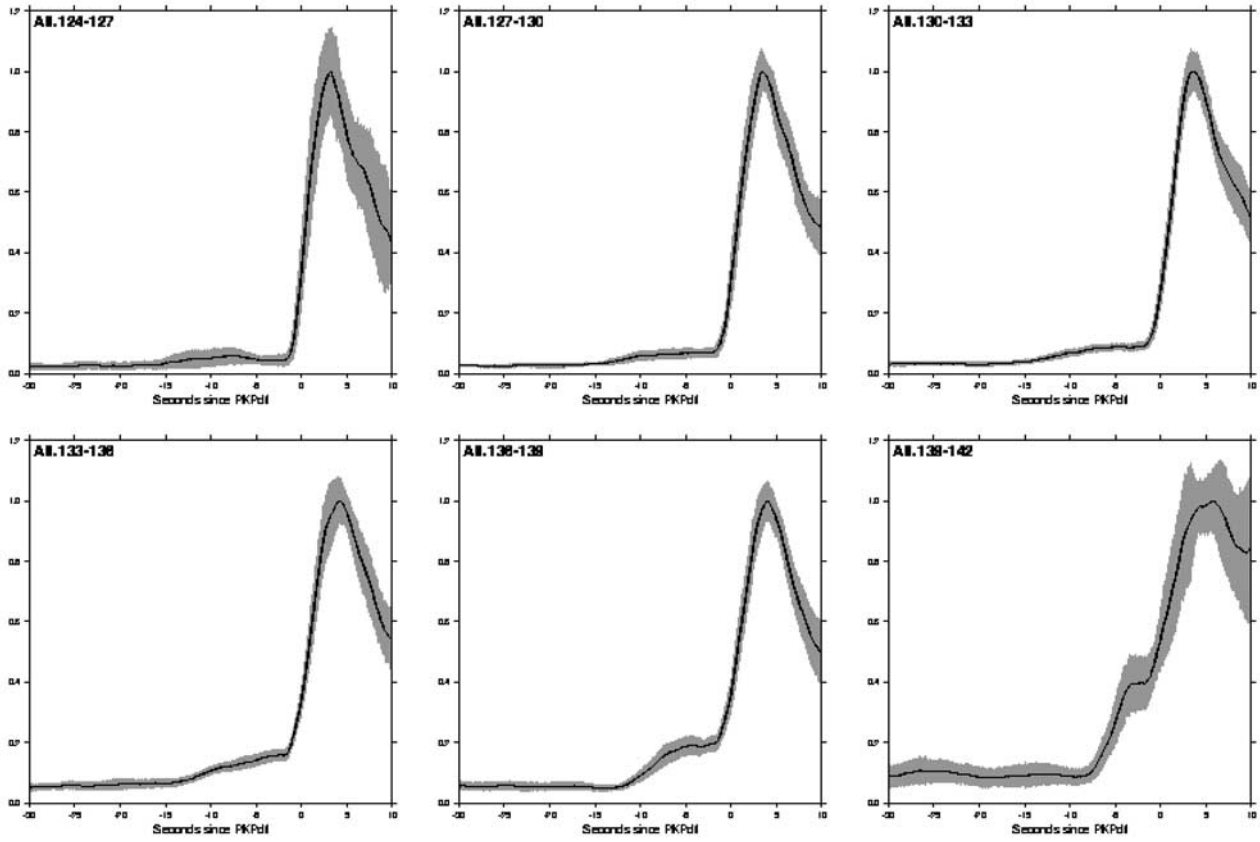

Figure 6. Stacked envelopes (with 95% confidence interval indicated by grey shading) for all 205 envelopes.

intervals of epicentral distance (ranging from 124°–127° to 139°–142°) and stacked the envelopes in each window.

[16] We experimented with different weighting of the stacks, and investigated both averaging the energies, or the RMS amplitudes directly. For the distance windows where we have sufficient data, these different computations yield essentially the same result. We finally opted for the technique that gave the lowest overall variance in the averages, as measured by the bootstrap method described below: we stack RMS amplitudes, inversely weighted with the noise level as measured from a time window preceding the scattered signal on the seismogram.

[17] We used a bootstrap technique [*Tichelaar and Ruff*, 1989] to estimate the 95% confidence intervals for the stacks. These intervals are indicated by the grey areas in the plots that follow. The global stacks are given in Figure 6, and the regional stacks are given in Figures 7–10. In

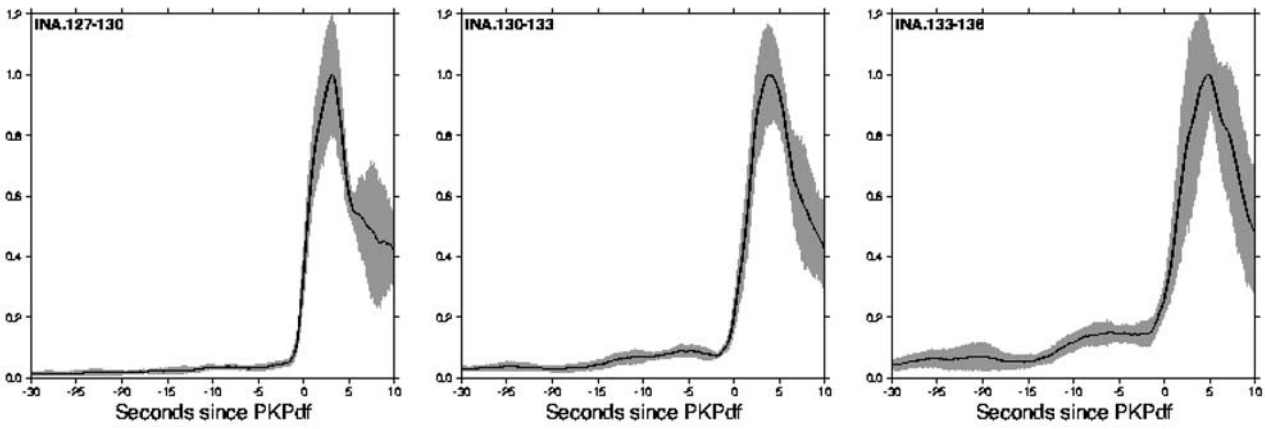

Figure 7. Stacked envelopes (with 95% confidence interval indicated by grey shading) for the Indonesia to North America corridor.

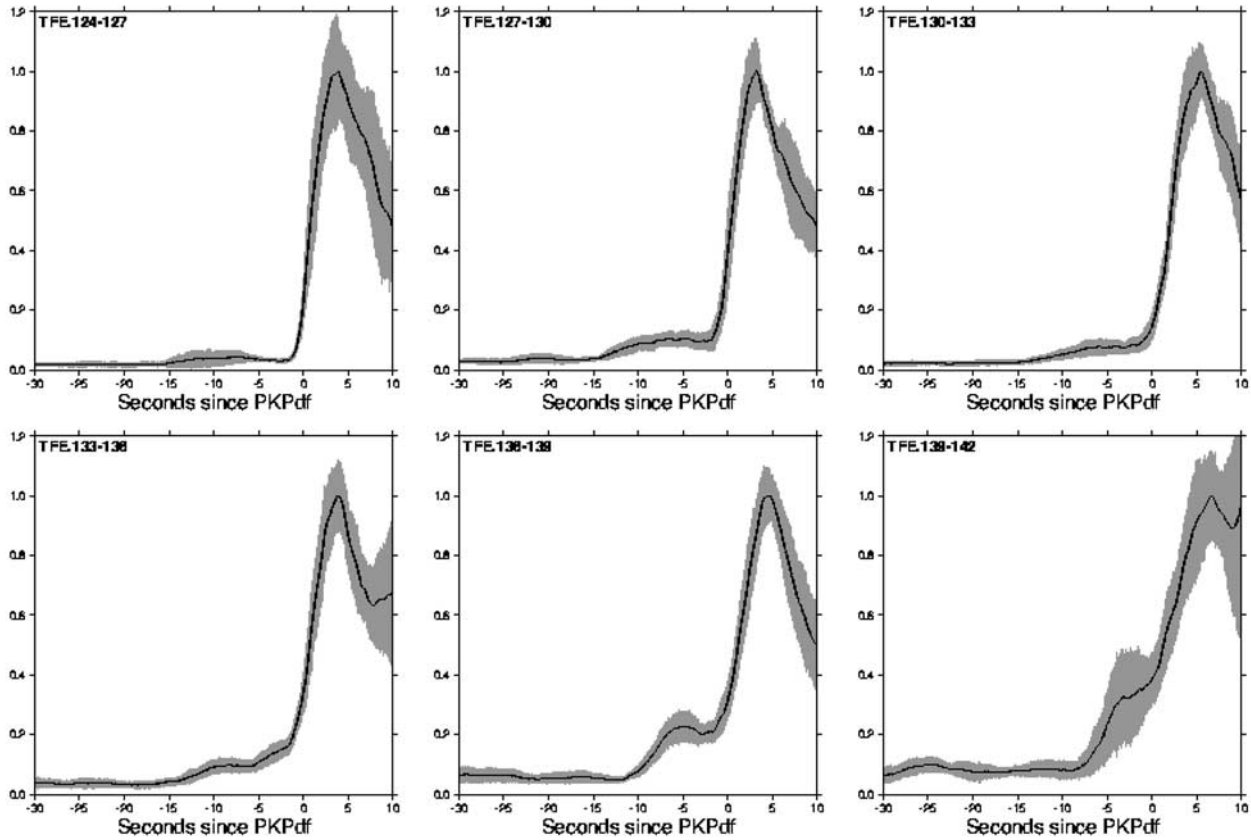

Figure 8. Stacked envelopes (with 95% confidence interval indicated by grey shading) for the Tonga-Fiji to North America corridor.

Figure 6, the RMS amplitude of the dominant inner core phases $PKP_{cd,df}$ has been normalized to 1 in each bin. The precursor energy gradually increases as the observer moves from short (124°) to large (142°) epicentral distances, thereby reflecting very clearly the scattering anisotropy. While the origin of the coda is ambiguous (it may be generated in the crust or at depth), the precursors would not exist without inhomogeneities at depth, and they carry information about the distribution of this heterogeneity. As will be illustrated in section 6, the decay rate of the scattered energy into the shadow zone is directly controlled by the power spectrum of the fluctuations.

[18] Figures 7–10 illustrate that for all corridors except for Tonga-Fiji to Eurasia (TFE), the range of observation of the precursors is only partially covered. Indeed, the bootstrap tests evidence that the global stack is slightly dominated by

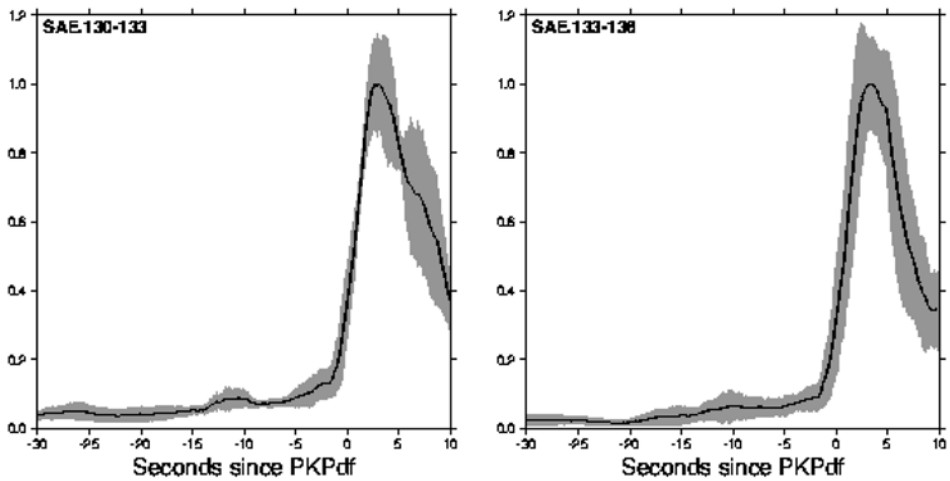

Figure 9. Stacked envelopes (with 95% confidence interval indicated by grey shading) for the South America to Eurasia corridor.

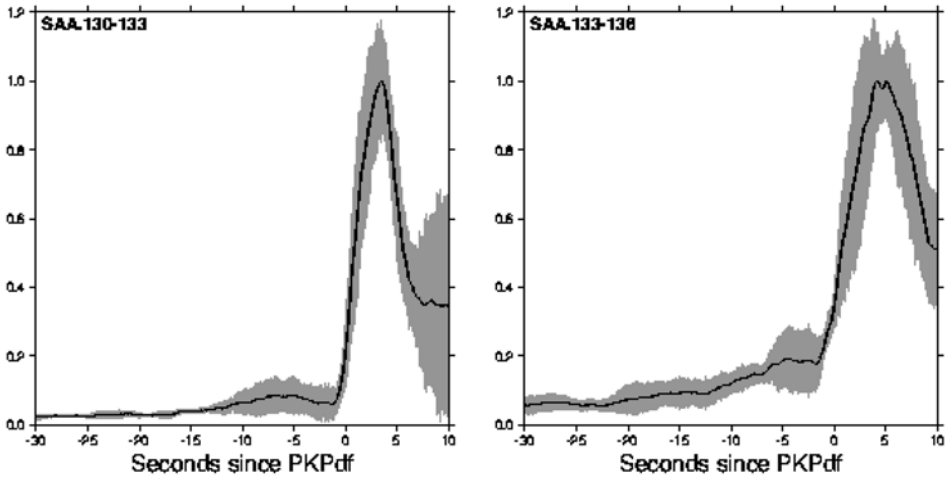

Figure 10. Stacked envelopes (with 95% confidence interval indicated by grey shading) for the South America to Australia corridor.

the TFE paths. The main interest in summing contributions from all paths is to average out some residual interferences, thereby reducing the uncertainty of our measurements. The interpretation of the global stack will be the focus of the rest of the paper. While of major interest for future work, a study of regional variations would distract us from our specific aim, which is to define the general characteristics of small-scale heterogeneities. We examine the inversion procedure in section 4 and refer the reader to RT-I for a detailed account of the forward modeling technique.

4. Inversion Method

4.1. Parameterization

[19] There are a number of factors that affect the range-time dependence of precursor amplitudes that we enumerate as follows:

[20] 1. A crucial parameter is the power spectrum of heterogeneities or the correlation function of the fluctuations, the two being Fourier transform pairs. This already offers an infinite number of degrees of freedom. As is customary, the analytical form of the correlations will be chosen a priori, leaving us with only two free parameters: the mean square fluctuations $\langle \epsilon^2 \rangle$ and the correlation length a. We shall find that this tremendous simplification suffices for our purposes. RT-I showed that the wave attenuation and the strength of the scattering are conveniently measured by a single parameter denoted by τ and termed the scattering mean free time. It can be understood as the statistical mean time between two scattering events. In the context of transport theory, the mean free time is a natural parameter because it appears directly in the governing equations. The inversion will thus be conducted in the (τ, a) parameter space. To ease comparison with other studies, we will translate the mean free time into RMS perturbations when necessary.

[21] 2. The thickness of the scattering layer plays a fundamental role. This parameter has a direct impact on the duration of the precursors and on the importance of multiple scattering. As explained in RT-I, waves are all the more prone to multiple interactions as the propagation length inside the heterogeneous medium increases. In the following we will put to the test D'' scattering models, where heterogeneities are restricted to the first 150 km above the CMB, and whole mantle scattering models where heterogeneities are distributed throughout the lower mantle.

[22] 3. The inner core intrinsic quality factor Q_c requires careful consideration. Since precursors stem from the scattering of PKP_{abc} waves which do not visit the inner core, Q_c has no effect on the precursor amplitude. However, because PKP_{df} plays the role of reference phase, any factor that affects its amplitude will modify our inference on the length scale and strength of inhomogeneities. In a first step, we adopt the PREM-like value $Q_c = 400$ but other possible values will be discussed in connection with recent work by *Li and Cormier* [2002] and *Cormier and Li* [2002].

4.2. Fitting Envelopes

[23] If we compute the solution of the transport equation for a point source in both space and time, we find that the seismogram envelopes look rather different from the observations. This discrepancy can be ascribed to the following effects: (1) the real source time function of earthquakes with magnitude 6 or higher, which is likely to last more than 5 s, and (2) the response of the crust produces scattered waves and reverberations that tend to spread the energy of incident waves in time. Although it would be desirable to disentangle the two causes, this would require a knowledge of the local small-scale structure, which remains unavailable. Even so, this issue is may be an order of magnitude more difficult than the original question. Aware of this fact, we adopted a pragmatic strategy, which consists in identifying the source time function by deconvolving the observed envelope of PKP_{cd} + PKP_{df} by the theoretically predicted envelope of the main phases in the 124°–127° epicentral distance range. This particular bin is preferable because the shape of the dominant pulse is unlikely to be affected by the precursors energy. We validate this procedure by verifying that the convolution of the theoretical impulse response with the inferred source function predicts adequately the typical duration of the dominant phases at all epicentral distances.

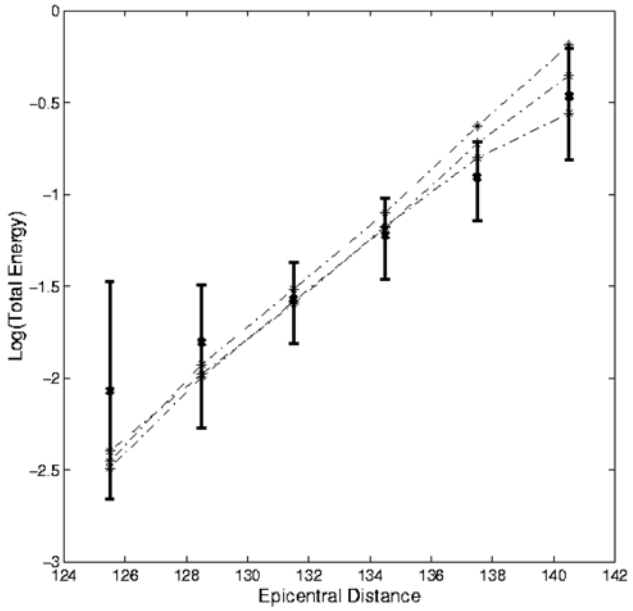

Figure 11. Total energy of the precursors as a function of epicentral distance. Solid line with error bars denotes data; Dashed lines denote best fitting models for D'' scattering and exponential correlation. The three lines correspond to the following pairs (mean free time, scale length): (400 s, 16 km), (800 s, 12 km), and (1600 s, 8 km). The data uncertainties are given by the 95% confidence interval of the bootstrap. Note that the energy is normalized with respect to the main phases (cd + df).

[24] In order to assess the agreement between a particular model and the observations, we use a simple χ^2 fitting method, where χ^2 is defined as

$$\chi^2 = \frac{1}{N}\sum_{i=1}^{N}\left(\frac{d(t_i) - y(a,\tau,t_i)}{\sigma(t_i)}\right)^2, \qquad (3)$$

where $d(t_i)$ is the observed amplitude at time t_i, σ is a typical uncertainty of the measurements, $y(a, \tau, t_i)$ is the modeled amplitude for a given value of correlation lengths and mean free time, and the sum runs over all data points in the time window of the precursors. As explained above, the thickness of the scattering layer and the inner core Q are fixed a priori. We emphasize that we do not try to invert simultaneously for the source time function and the scattering parameters. The source function is determined before the computation of the χ^2 with a method that uses direct waves only (see preceding paragraph). Also note that before computing the χ^2, the data are corrected for the noise level before the event. Since we are mainly interested in defining a set of possible models, we explore the (τ, a) parameter space with a grid search technique. It will also be found in section 5 that a simple by eye inspection of the envelopes suffices to reject without ambiguities a class of models.

5. D'' or Whole Mantle?

[25] The simplest observation that we need to explain is the increase of the time integrated energy of the precursors from 124° to 142° epicentral distance. In Figure 11, the thick black line shows the total precursor energy with typical uncertainties, while the dashed lines denote the three best fitting models for D'' scattering and exponential correlations. Figure 11 has been obtained by exploring a set of 49 models with correlation lengths [4, 5, 8, 12, 16, 20, 24] km and mean free times [50, 100, 200, 400, 800, 1600, 3200] s. Although the D'' hypothesis predicts a rate of decay which is faster than observed, the uncertainties in energy measurements alone do not allow us to conclusively reject this model. If we do the same exercise for whole mantle scattering models as illustrated in Figure 12, we clearly find a degradation of the agreement between observations and theoretical predictions. Indeed, the rate of change of the precursors energy with epicentral distance is clearly too rapid. From the sole consideration of the integrated energy, we may conclude that the D'' hypothesis should prevail.

[26] However, a more detailed analysis of time domain fits undoubtedly rules out D'' as the unique reservoir of heterogeneities in the lower mantle. In Figure 13, we show the range-time dependence of the precursor amplitude for different epicentral distances indicated on top of each plot. The dashed lines denote the mean amplitude of the data, while the thick lines show the best fitting model. The wiggly lines delimit the 95% confidence interval of the bootstrap. We first consider the case of exponential correlations and D'' scattering with the same 49 (τ, a) pairs as discussed previously. Although in certain epicentral distance ranges (124–127°,

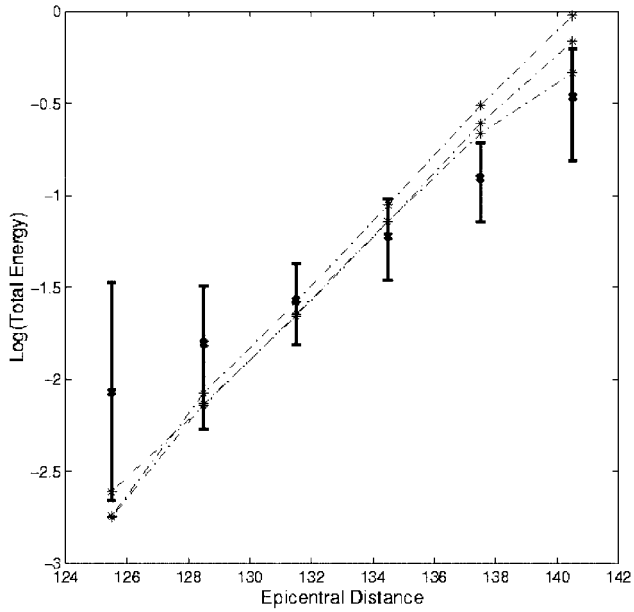

Figure 12. Total energy of the precursors as a function of epicentral distance. Symbols with error bars represents data; Dashed lines denote best fitting models with whole mantle scattering and exponential correlation. The three lines correspond to the following pairs (mean free time, scale length): (800 s, 20 km), (1600 s, 16 km), and (3200 s, 8 km). The data uncertainties are given by the 95% confidence interval of the bootstrap. Note that the energy has been normalized with respect to the main phases (cd + df).

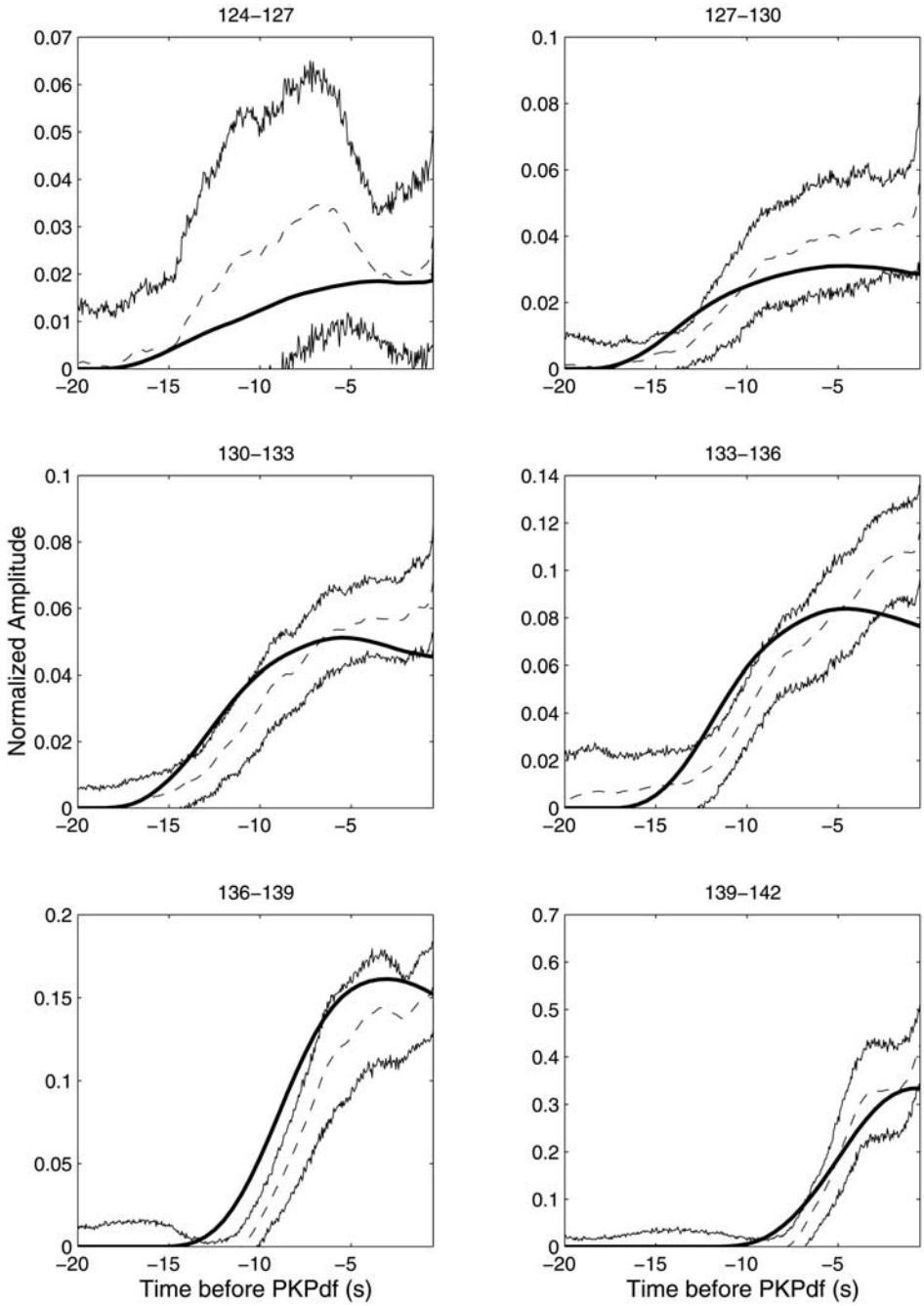

Figure 13. Time domain fits of precursors amplitudes for exponential correlations and D'' scattering. The dashed and thick lines denote the observed and modeled precursors amplitudes as a function of time before PKP_{df}. The peak PKP_{df} amplitude has been normalized to 1 in each epicentral distance bin, indicated on top of each plot. The wiggly lines delimit the 95% confidence interval of the bootstrap. The best fitting mean free time and correlation length are 800 s and 12 km, respectively.

139–142°), we find decent agreement between model and data, the predicted onset of the precursors in the intermediate epicentral distance range (130–133°, 133–136°) is much faster than observed. Moreover, the D'' model predicts a decay of the precursor amplitudes that occurs at times where the data still show a steady increase of the amplitude. These features were put forward by *Hedlin et al.* [1997] as the main reasons for rejecting the D'' hypothesis. Figure 14 illustrates the time domain fits for exponential correlations and whole mantle scattering. Although the predicted amplitude are too small in the deep shadow zone (124–127°, 127–130°) and too large close to the caustic (136–139°), whole mantle scattering models capture extremely well the overall time dependence of the precursors energy at intermediate distances. Notably, the onset time and duration of the data are now correctly reproduced. In agreement with previous findings

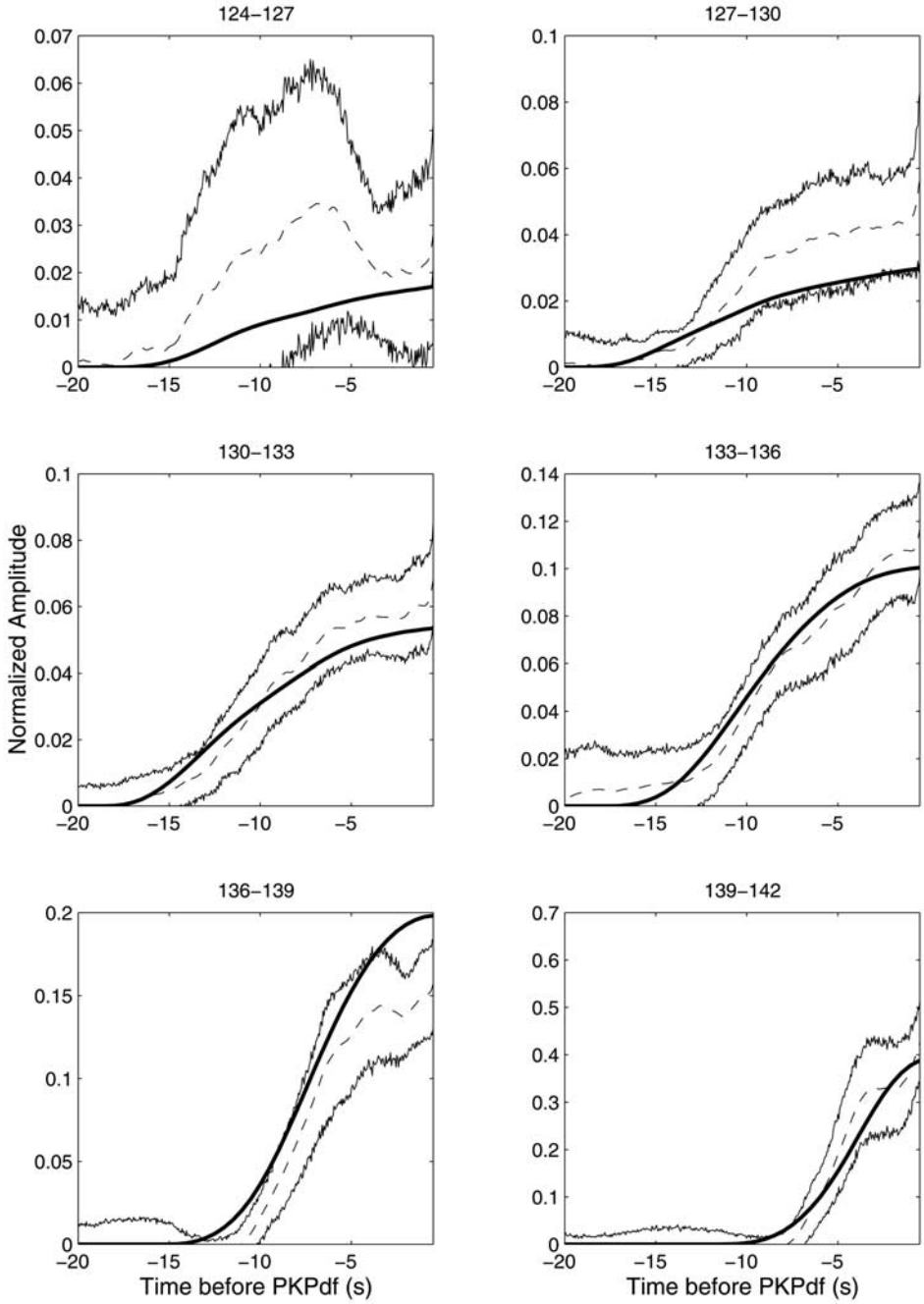

Figure 14. Time domain fits of precursors amplitudes for exponential correlations and whole mantle scattering. The best fitting mean free time and correlation length are 3200 s and 8 km, respectively. The rest is similar to Figure 13.

by *Hedlin et al.* [1997], we prefer the whole mantle scattering hypothesis. It is to be noted that our best fits are achieved for mean free times and correlation lengths in the [800, 3200] and [8, 20] km ranges, respectively. These scattering parameters correspond to very moderate RMS perturbations of the order of 0.25%, which is much lower than what has been proposed by Hedlin et al. The origin of this discrepancy will be further discussed at the end of the paper.

[27] Figures 12 and 14 demonstrate that the fits obtained with exponential correlations are not uniform. Typically, if we try to adjust the (τ, a) parameters in order to increase the amplitudes at short epicentral distances (124–127°), we systematically overpredict the amplitude close to the caustic. This feature of exponential correlations is extremely robust and does not depend on the assumed value of Q_c or on the thickness of the scattering layer, provided it is larger than about 600 km. This was also noticed by *Hedlin et al.* [1997]. Because the Born approximation has been shown to be a rather good workhorse for the weak perturbations invoked, it is clear that multiple scattering alone cannot reconcile data and observations. It may be argued that the nonuniformity of the fit is an artifact caused by the limited and uneven data

coverage. For example, some epicentral distances may be dominated by specific corridors that sample regions with perturbations stronger (or weaker) than the average. The fact that the observed discrepancy is systematic supports the idea that correlations in the lower mantle may be different from exponential. This alternative is explored in section 6.

6. Granularity of the Lower Mantle

[28] A well-known outcome of Born theory is the Booker and Gordon formula [*Ishimaru*, 1978] which relates the power spectrum of heterogeneities to the energy scattered by a unit volume of inhomogeneity at a certain angle. For acoustic scattering, this formula can be expressed as follows:

$$\sigma(\theta) \propto k^4 \Phi(q), \tag{4}$$

where θ denotes the scattering angle in polar coordinates, σ is the scattering cross section per unit volume, k is the wave number, $q = 2k\sin(\theta/2)$ is the magnitude of the scattering vector, and Φ is the power spectrum of the inhomogeneities. Note that the result is slightly more complex for elastic waves, but in the case of *P*-to-*P* scattering due to velocity perturbations, the acoustic approximation suffices. Formula (4) implies that the signals scattered at larger and larger angles (θ increases) sample shorter and shorter length scales of inhomogeneities (q increases). It is, in fact, well known that small-scale objects entail scattering at large angles. In the extreme case of point heterogeneities, the scattering of acoustic waves is perfectly isotropic. In the geometry of *PKP* precursors, the rapid decay of the precursors amplitude observed as one moves deeper and deeper into the shadow zone reflects the cutoff of large wave numbers in the power spectrum. As a consequence of scattering at different depths and possible multiple interactions, the correspondence between scattering angle and epicentral distance is not one to one, and our argument is to be considered as qualitative. However, this rule of thumb guided us in the choice of correlation function. Media with exponential correlation have the following power spectrum:

$$\Phi(q) = \frac{\langle \epsilon^2 \rangle a^3}{\pi^2 (1 + a^2 q^2)^2}, \tag{5}$$

where $\langle \epsilon^2 \rangle$ is the total variance of the velocity perturbations and a is the correlation length. For large q, Φ decays as q^{-4}. A simple way of increasing the amount of energy scattered at large angles in the shadow zone is to choose a correlation function which is richer in small scales. We therefore propose to use the following form of power spectrum:

$$\Phi(q) = \frac{\langle \epsilon^2 \rangle a^3}{4\pi (1 + a^2 q^2)^{3/2}}, \tag{6}$$

which corresponds to the following spatial correlation function C:

$$C(r) = \langle \epsilon^2 \rangle K_0\left(\frac{r}{a}\right), \tag{7}$$

where K_0 is a Bessel function of imaginary argument (see *Gradshtein and Ryzhik* [1979, p. 952] for definition).

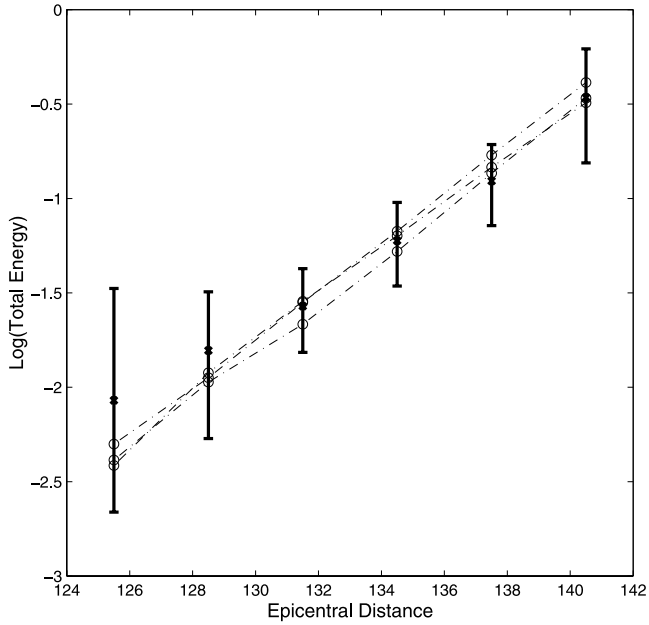

Figure 15. Total energy of the precursors as a function of epicentral distance. Solid line with error bars denotes data; Dashed lines denote best fitting models with whole mantle scattering and H-G correlation. The three lines correspond to the following pairs (mean free time, scale length): (800 s, 80 km), (1600 s, 30 km), (3200 s, 15 km). The data uncertainties are given by the 95% confidence interval of the bootstrap. Note that the energy is normalized with respect to the main phases (cd + df).

The angular dependence of the scattering in continuous random media having the power spectrum (6) is equivalent to what has been proposed in astrophysics by *Henyey and Greenstein* [1941] to describe light scattering by small discrete particles. In view of this resemblance, we term C in equation (7), the Henyey and Greenstein (H-G) correlation function. It can easily be seen that the H-G fluctuation model has infinite variance. Thus the usual interpretation of $\langle \epsilon^2 \rangle$ as the total variance of velocity fluctuations seems to be lost. The physical interpretation of $\langle \epsilon^2 \rangle$ will be discussed in great detail in section 7, when we translate the mean free time value into velocity perturbations.

[29] With the new H-G correlation function, we can carry out another inversion of the data following the steps presented in section 5. In Figure 15, we compare the observed and predicted dependence of the total precursor energy as a function of epicentral distance in the whole mantle scattering case. As expected, we find that the modeled rate of decay of the energy from the caustic to the deep shadow zone is in closer agreement with the observations. It is, however, noticable that the kink present in the data at an epicentral distance of about 132° is not reproduced by our simple statistical model. This kink has been previously noted by *Cormier* [1995, 1999] and seems to be a rather robust feature. Again, this may be due to a complicated spectrum of heterogeneities or to the dominance of certain paths with stronger perturbations in the data set. This issue will be further discussed in section 7. In Figure 16, we show an example of time domain fit of precursors amplitude. The agreement appears reasonably

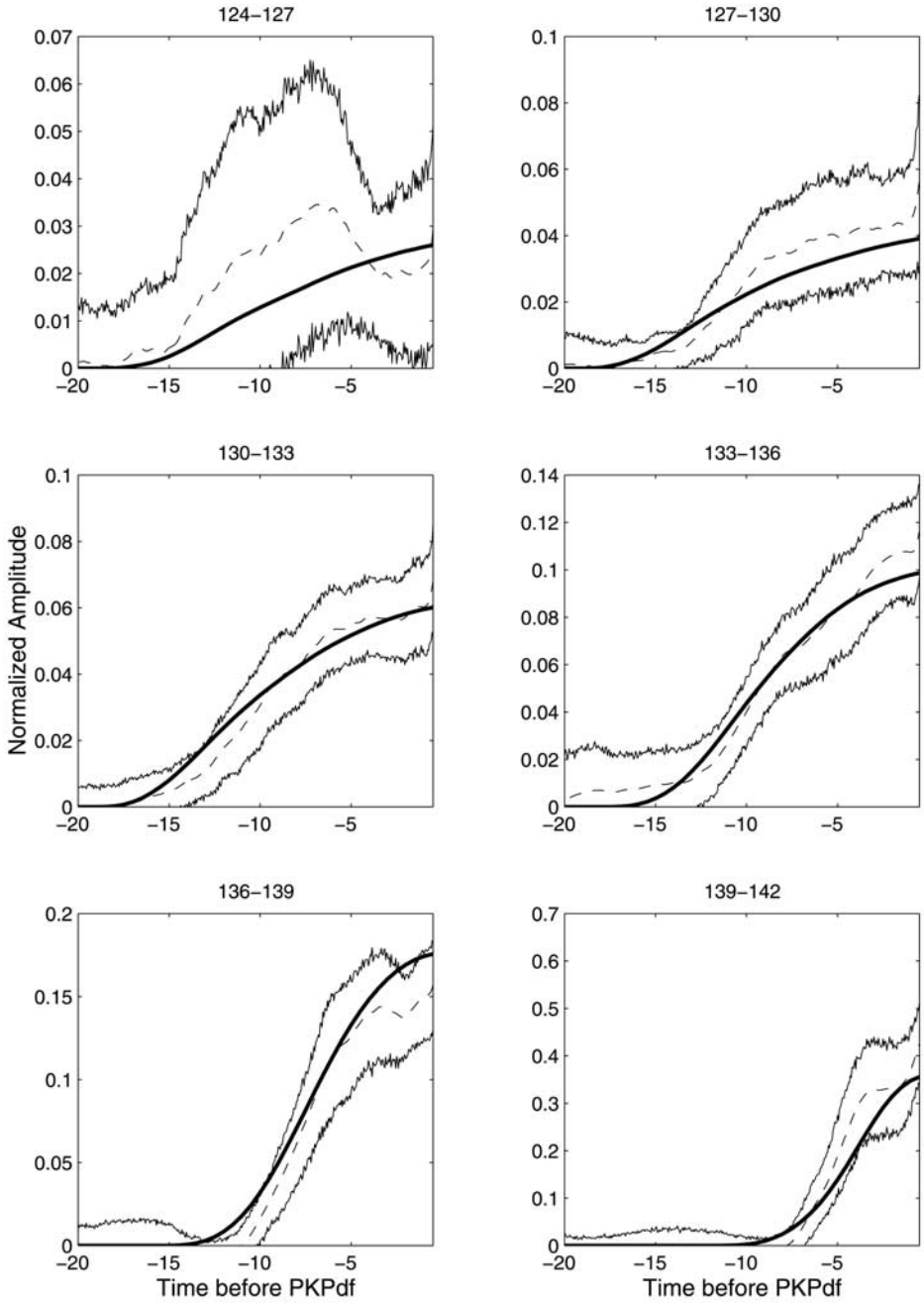

Figure 16. Time domain fits of precursors amplitudes for H-G correlations and whole mantle scattering. The best fitting mean free time and correlation length are 1600 s and 30 km, respectively. The rest is similar to Figure 13.

good at all epicentral distance bins simultaneously. Thereby, we achieve our goal of fitting uniformly the data, and confirm that an inhomogeneous layer of at least 600 km seems required to explain the *PKP* precursors. A novel finding is the strong irregularity of the medium implied by the richness in small-scale features in H-G random media.

7. Discussion and Conclusion

7.1. Nonunicity of the Inversion

[30] It is worth mentioning that the same quality of fit can be achieved by several models located on a trade-off curve in the (τ, a) plane. This point is illustrated in Figure 17, where we show a contour plot of the χ^2 for the different models with H-G correlation that were investigated. The reader may wonder why the length scales are unevenly sampled (see vertical axis). The reason is that in media with H-G correlations, the angular dependence of the scattering does not change linearly with the length scale. As explained in RT-I, the degree of scattering anisotropy can be quantified in a simple way by an anisotropy parameter denoted by g, which depends on the mean cosine of the scattering angle. The set of values adopted for the correlation length corresponds to a regular sampling in g space, which ensures

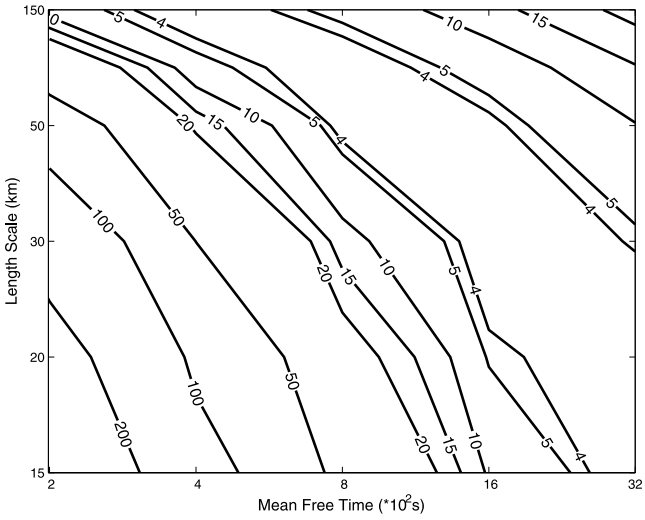

Figure 17. Contour plot of χ^2 as a function of mean free time (horizontal axis) and correlation length (vertical axis) for H-G correlations. The best fitting models are all located in a well-defined region of minimum χ^2. The horizontal axis uses a logarithmic scale. The scale on the vertical axis is linear in scattering anisotropy parameter g but nonlinear in length scales (see text for details).

that in each model the scattering pattern changes significantly. From Figure 17 we conclude that a correlation length of inhomogeneity cannot be extracted from our data. It is very likely that this is a consequence of the limited range of observation. In particular, equations (4) and (6) predict that at small scattering angles (small q), the scattered energy reaches a plateau. The observation of this plateau would provide an estimate of the correlation length. Unfortunately, in our geometry, small scattering angles correspond mostly to diffracted waves that arrive very close to the caustic where all the different phases interfere simultaneously. In this region, the measurements are extremely difficult and doomed to be highly inaccurate. Our inability to observe the precursors in the close neighborhood of the caustic probably explains why the trade-off between mean free time and correlation length cannot be resolved.

7.2. Inner Core Anelasticity

[31] In view of recent work by *Cormier and Li* [2002], we also tested lower values of inner core Q, of the order of 250. This tends to slightly translate rightward the trade-off curve in the (τ, a) plane, although the effect is relatively minor. The fits are slightly worse in this case because the amplitude of PKP_{df} is rather strongly affected close to the caustic. A way to correct for this would be to choose an even more irregular type of random medium. We did not try to do so in as much as the values of attenuation in the inner core are still actively debated. Also, one may argue that if attenuation is dominated by scattering, the part of the energy diffracted by the inner core is not irreversibly lost but may instead be present in the coda of PKP_{df}. Because we convolve our results with a source function that spans a few seconds, inner core scattering is not to be considered as a loss.

7.3. Effect of Noise

[32] In section 7.2, we noted that the variation of data amplitude as a function of epicentral distance exhibits a small but visible change of slope at about 132° epicentral distance. Here, we examine more quantitatively the reliability of this observation. As the energy of the scattered waves diminishes from the caustic to the shadow zone, more and more seismograms will be rejected because of low signal-to-noise ratio. Rejecting seismograms implies that the measured intensity is somehow biased toward values higher than the statistical mean in absence of noise. In order to quantify this effect, let us introduce some notations: $\langle N \rangle$, the mean noise energy; $\langle I \rangle$, the unbiased intensity, i.e., the intensity that would be measured in absence of noise; and $\langle I \rangle_{\text{obs}}$, the observed mean energy of the data. Let us make the reasonable assumption that the scattered wave field is a sum of many independent waves with uncorrelated amplitudes and phases. It is then possible to show (see *Goodman* [1985] or *Sheng* [1995]) that the resulting intensity I is distributed exponentially:

$$P(i \le I < i + di) = \frac{1}{\langle I \rangle} e^{-i/\langle I \rangle} di. \tag{8}$$

In practical data analysis, a precursor will be detected, provided its energy is larger than α times the noise level. Thus the noise prevents us from observing the complete probability distribution of intensities. This implies that $\langle I \rangle_{\text{obs}}$ is a biased statistical average for values of intensities larger than $\alpha \langle N \rangle$:

$$\langle I \rangle_{\text{obs}} = \frac{\int_{\alpha N}^{\infty} \frac{i}{\langle I \rangle} e^{-i/\langle I \rangle} di}{\int_{\alpha N}^{\infty} \frac{1}{\langle I \rangle} e^{-i/\langle I \rangle} di}. \tag{9}$$

After carrying out the integrations, one obtains

$$\langle I \rangle_{\text{obs}} = \langle I \rangle + \alpha \langle N \rangle. \tag{10}$$

This formula may indeed explain the kink in the data curves in log scale (see, e.g., Figure 11), provided $\alpha N \approx \langle I \rangle$ around 130° epicentral distance.

7.4. Physical Interpretation of $\langle \epsilon^2 \rangle$

[33] Finally, it is interesting to translate the values of mean free time in terms of strength of perturbations. At this point it is important to discuss the physical interpretation of the parameter $\langle \epsilon^2 \rangle$ that appears in the definition of any correlation function. As noted above, because the Bessel function diverges at $r = 0$, the total variance of media with H-G correlations is infinite. This is not the only type of correlation functions with infinite variance. One of the most popular models in scattering theory is the delta correlation model, where the correlation function is a Dirac delta distribution. At first sight these models look unphysical, but they all do yield perfectly well-defined scattering parameters, whether one is using Born approximation or more sophisticated scattering theories such as radiative

transfer. For example, the scattering mean free path l for acoustic waves with central wave number k reads

$$l^{-1} = \frac{k^4\pi}{2} \int_{4\pi} \Phi\left(2k \sin\frac{\theta}{2}\right) d\Omega, \tag{11}$$

where the integration is over the whole sphere of space direction. Equation (11) nicely shows that the mean free path depends only on the power spectrum of the fluctuations ϕ in the range $[0, 2k]$. The Booker and Gordon formula (4) likewise illustrates that the singly scattered intensity can only yield information on the power spectrum in the same interval. Ideally, one would need to probe the medium with waves of arbitrarily high frequencies to recover the whole fluctuation spectrum. In practice, this is never the case, and the correlation functions are only idealizations of the true medium that are valid only in a finite wave number band. The calculation of the total variance requires integration from 0 to $+\infty$ and gives an enormous weight to infinitely small-scale features which are fundamentally unresolvable by finite frequency waves. Therefore the divergence of the total variance is a purely mathematical artifact. For waves with central wave number k, one should instead define a physical or "wave" variance as

$$\langle \epsilon^2 \rangle_{\text{wave}} = 4\pi \int_0^{2k} \Phi(k) k^2 dk, \tag{12}$$

where the prefactor comes from an integration over angular variables. This parameter is always finite but differs from the usual $\langle \epsilon^2 \rangle$. For exponential and H-G correlations, one finds

$$\langle \epsilon^2 \rangle_{\text{wave}} = \frac{2\langle \epsilon^2 \rangle}{\pi} \left[\tan^{-1}(2ka) - \frac{2ka}{(1+4k^2a^2)} \right], \tag{13}$$

and

$$\langle \epsilon^2 \rangle_{\text{wave}} = \frac{\langle \epsilon^2 \rangle}{4\pi} \left[\sinh^{-1}(2ka) - \frac{2ka}{(1+4k^2a^2)^{1/2}} \right], \tag{14}$$

respectively.

[34] Note that for exponential media, $\langle \epsilon^2 \rangle_{\text{wave}}$ and $\langle \epsilon^2 \rangle$ differ by no more than 15%, for $ka > 5$, which is typically the case in this study. The above discussion should make it clear that the total variance is actually not the most relevant parameter to describe a scattering model. As emphasized above, the mean free path/time can be calculated for any correlation function and should therefore be adopted as the key parameter.

[35] Let us nevertheless calculate the value of $\epsilon^2{}_{\text{wave}}$ for the best fitting H-G media. For a simple model with pure P wave velocity perturbations the exact expression of the mean free time in media with H-G correlation reads [e.g., *Ishimaru*, 1978]:

$$\tau^{-1} = \pi k^2 a \langle \epsilon^2 \rangle \alpha \left[1 - \left(1 + 4k^2a^2\right)^{-1/2} \right], \tag{15}$$

where α denotes the local P wave speed. For H-G correlation, we find that extremely weak perturbations (defined as the square root of $\langle \epsilon^2 \rangle_{\text{wave}}$) of order 0.1% suffice to explain the precursor amplitudes, independent of the length scale. For exponential correlations, the required perturbations are slightly higher, of order 0.25%. Because our stacks comprise only the clearly visible signals, they probably correspond to the most energetic precursors analyzed by Hedlin's group, for which perturbations of up to 2% were invoked. Our value is smaller by a factor 10–20, which represents a tremendous difference in terms of wave attenuation. Note that according to the preceding discussion, the comparison of perturbations between the two studies can be considered as meaningful for exponential media only. This large discrepancy cannot find its origin in multiple-scattering effects because the weakness of the perturbations in our model guarantees that high-order scatterings are very unlikely. The difference in modeling techniques is the most probable explanation for the different estimates, but the problem is still open.

[36] In conclusion, a new method of study of high-frequency seismic waves based on the modern theory of radiative transfer has been developed and applied to the modeling of *PKP* precursors. Our investigations confirm that small-scale heterogeneities are very likely to be present at a wide range of depth in the lower mantle. A simple inversion reveals that the limited range of observation does not allow an estimation of the correlation length of the fluctuations. We believe that the typical size of 8 km previously proposed is unjustified. However, it seems possible to extract the slope of the decay of the power spectrum of heterogeneities from the decrease of the precursor amplitudes observed from the caustic to the deep shadow zone. This leads us to propose a model of the mantle which contains tiny but very irregular fluctuations that enable a uniform fit of the data. The strength of fluctuations required to explain our data set is of order 0.1–0.2% which constitutes a major difference with previous investigations. The explanation of this discrepancy remains largely an open question. To solve this issue, we propose to apply in the near future the theory of radiative transfer to the modeling of the coda of other seismic phases.

[37] **Acknowledgments.** The authors would like to thank M. Hedlin and P. Shearer for reviewing an early version of this manuscript and providing many helpful suggestions and comments. We are grateful to H. Sato for pointing out an important question regarding the physical meaning of $\langle \epsilon^2 \rangle$. The authors benefited from discussions and encouragements from F. A. Dahlen in the course of this work. Discussions with N. Shapiro, P. Earle, V. Cormier, and J. R. Grasso were also greatly appreciated. This research was partially supported by the National Science Foundation (grant EAR-0003348), and the French Ministry of Research (ACI "jeune chercheur").

References

Apresyan, L. A., and Y. A. Kravtsov, *Radiation Transfer: Statistical and Wave Aspects*, Gordon and Breach, Newark N.J., 1996.

Barabanenkov, Y., A. Vinogradov, Y. Kravtsov, and V. Tatarskii, Application of the theory of multiple scattering of waves to the derivation of the radiative transfer equation for a statistically inhomogeneous medium, *Radiofizika*, *15*, 1852–1860, 1972.

Bolt, B. A., Gutenberg's early *PKP* observations, *Nature*, *196*, 122–124, 1962.

Buffett, B., R. Jeanloz, and E. Garnero, Sediments at the top of the Earth's core, *Science*, *288*, 2007–2012, 2000.

Cleary, J. R., and R. A. W. Haddon, Seismic wave scattering near the core-mantle boundary: A new interpretation of precursors to *PKP*, *Nature*, *240*, 549–551, 1972.

Cormier, V. F., Time-domain modelling of *PKIKP* precursors for constraints on the heterogeneity in the lowermost mantle, *Geophys. J. Int.*, *121*, 725–736, 1995.

Cormier, V. F., Anisotropy of heterogeneity scale lengths in the lower mantle from *PKIKP* precursors, *Geophys. J. Int.*, *136*, 373–384, 1999.

Cormier, V. F., and X. Li, Frequency-dependent seismic attenuation in the inner core: 2. A scattering and fabric interpretation, *J. Geophys. Res.*, *107*(B12), 2362, doi:10.1029/2002JB001796, 2002.

Dahlen, F. A., S.-H. Hung, and G. Nolet, Frechet kernels for finite-frequency traveltimes-I. Theory, *Geophys. J. Int.*, *141*, 157–174, 2000.

Doornbos, D. J., Characteristics of lower mantle inhomogeneities from scattered waves, *Geophys. J. R. Astron. Soc.*, *53*, 643–663, 1976.

Doornbos, D. J., On seismic wave scattering by a rough core mantle boundary, *Geophys. J. R. Astron. Soc.*, *53*, 643–662, 1978.

Doornbos, D. J., and E. S. Husebeye, Array analysis of *PKP* phases and their precursors, *Phys. Earth Planet. Inter.*, *5*, 387, 1972.

Doornbos, D. J., and N. J. Vlaar, Regions of seismic wave scattering in the Earth's mantle and precursors to *PKP*, *Nature Phys. Sci.*, *243*, 58–61, 1973.

Goodman, J. W., *Statistical Optics*, John Wiley, Hoboken, N. J., 1985.

Gradshtein, I. S., and I. M. Ryzhik, *Table of Integrals, Series, and Products*, corrected and enlarged edition, Academic, San Diego, Calif., 1979.

Haddon, R. A. W., and J. R. Cleary, Evidence for scattering of seismic PKP waves near the mantle-core boundary, *Phys. Earth Planet. Inter.*, *8*, 211–234, 1974.

Hansen, J. E., and J. W. Hovenier, Interpretation of the polarization of Venus, *J. Atmos. Sci.*, *27*, 265–281, 1974.

Hedlin, M. A. H., and P. Shearer, An analysis of large-scale variations in small-scale mantle heterogeneity using Global Seismographic Network recordings of precursors to *PKP*, *J. Geophys. Res.*, *105*, 13,655–13,673, 2000.

Hedlin, M. A. H., P. Shearer, and P. S. Earle, Seismic evidence for small-scale heterogeneity throughout the Earth's mantle, *Nature*, *387*, 145–150, 1997.

Henyey, L., and J. Greenstein, Diffuse radiation in the galaxy, *Astrophys. J.*, *93*, 70–83, 1941.

Hung, S.-H., F. A. Dahlen, and G. Nolet, Frechet kernels for finite-frequency traveltimes-II. Examples, *Geophys. J. Int.*, *141*, 175–203, 2000.

Husebeye, E. S., D. W. King, and R. A. W. Haddon, Precursors to *PKIKP* and seismic wave scattering near the mantle-core boundary, *J. Geophys. Res.*, *81*, 1870–1882, 1976.

Ishimaru, A., *Wave Propagation and Scattering in Random Media*, vols. I and II, Academic, San Diego, Calif., 1978.

King, D. W., R. A. W. Haddon, and J. R. Cleary, Array analysis of precursors to *PKIKP* in the distance range 128° to 142°, *Geophys. J. R. Astron. Soc.*, *37*, 157–173, 1974.

Li, X., and V. F. Cormier, Frequency-dependent seismic attenuation in the inner core: 1. A viscoelastic interpretation, *J. Geophys. Res.*, *107*(B12), 2361, doi:10.1029/2002JB001795, 2002.

Margerin, L., and G. Nolet, Multiple scattering of high-frequency seismic waves in the deep Earth: Modeling and numerical examples, *J. Geophys. Res.*, *108*(B5), 2234, doi:10.1029/2002JB001974, 2003.

Nolet, G., and F. A. Dahlen, Wave front healing and the evolution of seismic delay times, *J. Geophys. Res.*, *105*, 19,043–19,054, 2000.

Rytov, S. M., Y. A. Kravtsov, and V. I. Tatarskii, *Principles of Statistical Radiophysics*, vol. 3, *Elements of Random Fields*, Springer-Verlag, New York, 1989a.

Rytov, S. M., Y. A. Kravtsov, and V. I. Tatarskii, *Principles of Statistical Radiophysics*, vol. 4, *Wave Propagation Through Random Media*, Springer-Verlag, New York, 1989b.

Ryzhik, L. V., G. C. Papanicolaou, and J. B. Keller, Transport equations for elastic and other waves in random media, *Wave Motion*, *24*, 327–370, 1996.

Sato, H., and M. Fehler, *Seismic Wave Propagation in the Heterogeneous Earth*, Springer-Verlag, New York, 1998.

Shearer, P. M., M. A. H. Hedlin, and P. Earle, *PKP* and *PKKP* precursor observations: Implications for the small-scale structure of the deep mantle and core, in *The Core-Mantle Boundary Region*, *Geodyn. Ser.*, vol. 28, edited by M. Gurnis et al., pp. 37–55, AGU, Washington, D. C., 1998.

Sheng, P., *Introduction to Wave Scattering, Localization and Mesoscopic Phenomena*, Academic, San Diego, Calif., 1995.

Tichelaar, B. W., and L. J. Ruff, How good are our best models?, *Eos Trans. AGU*, *70*, 593, 605–606, 1989.

Weaver, R. L., Diffusivity of ultrasound in polycrystals, *J. Mech. Phys. Solids*, *38*, 55–86, 1990.

L. Margerin, Laboratoire de Géophysique Interne et Tectonophysique, Observatoire de Grenoble, Université Joseph Fourier, BP 53X, 38041 Grenoble Cedex, France. (ludovic.margerin@lgit.obs.ujf-grenoble.fr)

G. Nolet, Department of Geosciences, Princeton University, Guyot Hall, Princeton, NJ 08544, USA. (nolet@princeton.edu)